Gas permeation in bi-soft segment poly(ester urethane urea) membranes for Membrane Blood Oxygenators

Gabriela Pon

Supervisors: Dr. Mónica Cristina Faria Besteiro and Dr. Pedro Jorge Rodrigues Morgado

November 2018

Abstract

Integral asymmetric and nonporous symmetric poly(ester urethane urea) membranes were synthesized by a modified version of the phase inversion technique and the solvent evaporation technique, respectively, where polyurethane (PUR) and polycaprolactone-diol (PCL) prepolymers were reacted with the solvents dimethyl formamide (DMF) and diethyl ether (DEE). Four casting solutions were prepared with PUR/PCL weight ratio of 90/10, polymer/solvent ratio of 65/35 and DMF/DEE ratios of 3/1 and 1/1, rendering integral asymmetric membranes, A31 and A11, and nonporous symmetric membranes, D31 and D11.

An existing gas permeation setup was optimized by increasing the volume of the receiving chamber and performing vacuum to the setup before the measurements. The results were highly reproducible and permitted the determination of the diffusion and solubility coefficients by the time lag method.

Similar permeances were obtained for the integral asymmetric and nonporous symmetric membranes: 0.12-0.13x$10^{-6}$$cm^3$/$cm^2$.s.cmHg for N_2, 0.32-0.35x$10^{-6}$$cm^3$/$cm^2$.s.cmHg for O_2 and 3.2-3.4x$10^{-6}$$cm^3$/$cm^2$.s.cmHg for CO_2. The permeability coefficients obtained for membrane D31 were: 8, 21 and 208 Barrer for N_2, O_2 and CO_2, respectively. The diffusion coefficients obtained by the time lag method were very similar for the three gases: 7.1-13.0x$10^{-7}$$cm^2$/s for N_2, 7.4-11.0x$10^{-7}$$cm^2$/s for O_2 and 7.5-12.2x$10^{-7}$$cm^2$/s for CO_2. The solubility coefficients obtained by the time lag method were: 0.07-0.08x$10^{-2}$$cm^3$/$cm^3$.cmHg for N_2, 0.20-0.25x$10^{-2}$$cm^3$/$cm^3$.cmHg for O_2 and 1.7-2.2x$10^{-2}$$cm^3$/$cm^3$.cmHg for CO_2, which were the same order of magnitude obtained by the barometric method. The solubility coefficient was found to be the controlling term in these membranes which led to the differences observed in the permeabilities of the gases.

Keywords: Gas permeation; Bi-soft segment polyurethanes; Integral asymmetric membranes; Membrane blood oxygenators; Time lag

1 Introduction

Extracorporeal membrane oxygenation (ECMO) allows patients to survive and heal from cardiopulmonary surgery, traumatic injury, infection or inflammation of the lungs and is also used as a bridge to lung transplant. The ECMO circuit mainly consists of a tubing that takes out the deoxygenated blood from the patient, a pump, an artificial lung, a heat exchanger and a tubing that returns the oxygenated blood to the patient. It is in the artificial lung, also referred to as Membrane Blood Oxygenator (MBO), where gas exchange occurs [1,2,3]. The present work is focused on the development on new membranes for MBOs.

The ideal MBO should be able to [4]: perform efficient gas exchange; be hemocompatible, avoiding hemolysis and protein denaturation; oxygenate up to 5 L/min of venous blood to 95-100% haemoglobin saturation for periods between some minutes till several hours; simultaneously, remove a certain level of CO_2 to avoid respiratory acidosis but also not too much to avoid alkalosis; have reasonable blood priming volume (1-4L); be simple and safe to use, clean and sterilizable. The MBO must deliver about 250 cm^3 (STP)/min of O_2 and remove about 200 cm^3 (STP)/min of CO_2. Blood flows of 2-4 L/min are required.

Nowadays, hollow fiber membrane oxygenators have become the standard of care for CPB and bedridden ECMO. Microporous polypropylene (PP) hollow fiber membrane oxygenators have gained popularity, as it brought numerous advantages such as low priming volume, smaller surface area, ease of priming, low transmembrane pressure and adequate gas exchange. However, they present a major disadvantage when it comes to long-term usage, which is plasma leakage through the micropores and, consequently, a decrease in gas exchange. Recently, a non-microporous hollow fiber oxygenator made from polymethylpentene (PMP) was released, which considerably decreased the plasma leakage occurrence [3,5].

Currently, many studies are being carried out to improve the hemocompatibility of membranes. Although anticoagulants are used, deposition of blood proteins may still occur after a few days, leading to device failure. In addition, the use of anticoagulants increases the risk for bleeding. In the present, most studies are focused on membrane surface modification/functionalization to enhance hemocompatibility.

Zhao and de Pinho [6] have synthesized bi-soft segment poly(ester urethane urea) membranes by introducing poly(butadienediol) (PBDO) as a second soft segment. The introduction of another soft segment further increases the versatility in the structure design of PU membranes due to different degrees of phase separation between the two soft segments and different degrees of phase segregation between the hard and soft segments. Studies by Queiroz and de Pinho [7,8] showed that a membrane containg 20 wt.% of PBDO had higher degree of cross-linking, showed phase separation of the two soft segments and had higher CO_2 permeability, dependant on the feed pressure, which ranged from 150 to 950 Barrer. A membrane containg 67 wt.% of PBDO had lower degree of cross-linking, was more homogeneous, as the two soft segments were highly dispersed in each other, and lower CO_2 permeability, which was also dependant on the feed pressure and ranged from 90 to 550 Barrer. It was reported that the increase of PBDO content in the membranes increases the mixing of the two soft segments and decreases the aggregation of the hard segments (urethane/urea groups).

The same group has synthesized bi-soft segment poly(ester urethane urea) membranes by introducing another soft segment, which is the polydimethylsiloxane (PDMS) [9]. Studies revealed that the membranes with PDMS content ranging from 25 to 75 wt.% showed phase separation of the two soft segments and that the hard segments form small aggregates somewhere in these two phases. It was also concluded that the increase in PDMS content from 25 to 75 wt.% led to the increase of permeabilities to CO_2 from 200 to 800 Barrer and O_2 from 30 to 120 Barrer. The higher permeability of the membrane containing 75 wt.% was regarded as being caused by the higher fraction of siloxane segments, lower degree of cross-linking and lower aggregation of urethane/urea groups.

Faria *et al*. have introduced polycaprolactone (PCL) as a second soft segment to poly(ester urethane urea) integral asymmetric membranes, which strongly improved the hemocompatibility [10,11,12], compared to the PU/PBDO and PU/PDMS membranes. Although CO_2 permeation fluxes were in the order of magnitude required for commercial membrane oxygenators, the results for O_2 were much below the requirements [13]. The membranes containing PCL content ranging from 0 to 15 wt.% were characterized by infrared spectroscopy and it was concluded that the urethane groups form hard segment aggregates dispersed in the soft segment phase and that this aggregation increases with the increase in PCL content. Gas permeation experiments performed by a photoacoustic system resulted in permeabilities to CO_2 that increased from 188 to 337 Barrer when PCL content increased from 0 to 10 wt.% and was the lowest for 15 wt.% PCL content, which was 113 Barrer. The permeability to O_2 was independent of PCL content and was between 10 and 11 Barrer. Therefore, the membrane that showed the highest CO_2 permeability is the one that contains 10 wt.% PCL and is characterized by the highest contribution of hydrogen bonding between urethane and urea hard segments [14].

Recently, Eusébio [15] built an experimental gas permeation setup capable of recording the evolution of the permeate pressure online at a constant temperature, in intervals of 1.3 seconds, with a precision better than 10 Pa. However, results showed low reproducibility and high uncertainty associated for more permeable membranes, possibly due to various factors such as the small size of the receiving chamber and the fact that vacuum wasn´t applied to the setup prior to the measurements. Furthermore, a transient state was not observed in measurements with O_2, which made it impossible to determine the diffusion and solubility coefficients for this gas by the time lag method. Therefore, the optimization of the gas permeation setup is one of the aims of this work, in order to obtain more precise measurements and to be able to determine the diffusion and solubility coefficients of O_2 and CO_2 by the time lag method.

Eusébio [15] synthesized various bi-soft segment poly(ester urethane urea) membranes with PCL by varying the polymer/solvent ratio, polymers ratio (PUR/PCL), solvents ratio (DMF/DEE) and solvent evaporation time. Gas permeation results for membranes prepared with 1 minute solvent evaporation time were not reproducible and had high uncertainty associated. The membrane that showed the most promising result was the membrane with 1/1 polymer/solvent ratio, 85/15 PUR/PCL ratio and 5 minutes of solvent evaporation time. The N_2, O_2, and CO_2 permeances obtained for this membrane were 0.004 x 10^{-5} cm^3/cm^2.s.cmHg, 0.015 x 10^{-5} cm^3/cm^2.s.cmHg and 0.13 x 10^{-5} cm^3/cm^2.s.cmHg, respectively. In this work, these bi-soft segment poly(ester urethane urea) membranes containing PCL were synthesized and measured in the optimized gas permeation setup.

2 Mass Transport Phenomena

2.1 Solution-diffusion model

The transport of a single gas through a dense, nonporous polymeric membrane can be described by the solution-diffusion model. Being the pressure difference across the membrane the driving force, the gas molecules dissolve in the upstream face of the membrane, diffuse across the membrane and desorb from the downstream face of the membrane. Thus, the permeability (P) is both a function of diffusivity (D) and solubility (S) [16]:

$$P = DS \qquad (1)$$

In the steady-state, the unidimensional diffusive flux is described by the Fick´s First Law of diffusion:

$$J_A = -D_A \frac{dC_A}{dx} \qquad (2)$$

where J_A is the flux of species A in the x direction and is proportional to the concentration gradient $\frac{dC_A}{dx}$. C_A is the concentration of species A in the membrane and D_A is a proportionality constant defined as the diffusion coefficient. To simplify the calculations, it was assumed that the Knudsen diffusion is controlling, so the diffusion coefficient becomes independent of the concentration. However, this only applies at low pressures.

Integrating Equation 2 over the thickness of the membrane, l, gives

$$J_A = \frac{D_A}{l}(C_{A0} - C_{Al}) \qquad (3)$$

where C_{A0} and C_{Al} are the concentrations of A in the membrane on the feed side and permeate side, respectively.

The solubility of gases in elastomers is very low and can be described by Henry´s Law, given by Equation 4, where the concentration inside the polymer, C, is proportional to the applied pressure, p.

$$C = Sp \qquad (4)$$

By applying Henry´s Law, the following relations can be established

$$S_A = \frac{C_{A0}}{p_f} = \frac{C_{Al}}{p_p} \qquad (5)$$

where S_A is the solubility coefficient of A, p_f is the pressure of the feed and p_p is the pressure of the permeate [17].

Combining Equations 3 and 5 gives the following expression

$$J_A = \frac{D_A S_A}{l}(p_f - p_p) \qquad (6)$$

Since the product $D_A S_A$ is equal to the permeability coefficient, P_A, Equation 6 can be written as

$$J_A = \frac{P_A}{l}(p_f - p_p) \qquad (7)$$

The permeability coefficient is commonly expressed in Barrer where

$$1\ Barrer = 10^{-10}\left(\frac{cm^3(STP)\ cm}{cm^2\ s\ cmHg}\right)$$

When the thickness is difficult to define, the pressure normalized flux or permeance, $\frac{P_A}{l}$, is used instead.

The ideal selectivity of the membrane, $\alpha_{A/B}$, is the ratio of the permeabilities or permeances of the individual gases. For a mixture of gas A and B the ideal selectivity is described by [16]:

$$\alpha_{A/B} = \frac{P_A}{P_B} \qquad (8)$$

2.2 Time lag method

In the transient-state, the mass balance of the unidimensional diffusive transport of species A through a dense, nonporous polymeric membrane is given by the following expression:

$$-\frac{dC_A}{dt} = \frac{dJ_A}{dx} \qquad (9)$$

Substituting the flux by the Fick´s First Law (Equation 2), the Fick´s Second Law is obtained:

$$\frac{dC_A}{dt} = D_A \frac{d^2 C_A}{dx^2} \qquad (10)$$

If the membrane is initially free of the diffusing species, the following initial and boundary conditions for the system can be applied:

$$C_A(x,0) = 0 \qquad (11.a)$$

$$C_A(0,t) = C_{A0} \qquad (11.b)$$

$$C_A(l,t) = C_{Al} \approx 0 \qquad (11.c)$$

which means that the upstream concentration, C_{A0}, remains constant and the downstream concentration, C_{Al}, is negligible compared to the upstream during the diffusion process. Fulfilling these boundary conditions, the solution of Equation 10, either by Laplace transform or separation of variables, is given by [18,19]:

$$C_A = C_{A0}\left(1 - \frac{x}{l}\right) + \frac{2C_{A0}}{l} \times \sum_{n=1}^{\infty} \frac{1}{n} \sin\left(\frac{n\pi x}{l}\right) exp\left(-\frac{D_A n^2 \pi^2 t}{l^2}\right) \qquad (12)$$

The solution expressed in terms of the diffusive flux can be obtained by substituting Equation 12 in the Fick´s First Law:

$$J_A(x,t) = \frac{D_A C_{A0}}{l} + \frac{2D_A C_{A0}}{l} \times \sum_{n=1}^{\infty} \cos\left(\frac{n\pi x}{l}\right) exp\left(-\frac{D_A n^2 \pi^2 t}{l^2}\right) \qquad (13)$$

The first term in Equation 13 is the steady state portion of the flux and the second term represents the transient contribution. It is a function of time and displacement in the direction of diffusion and hence can be solved for the fluxes entering and leaving the membrane ($x = 0$ and $x = l$, respectively).

By setting $x = l$, yields a time dependant flux equation relative to the downstream end of the membrane. Integrating it with respect to time, yields the amount of species A permeating out of the membrane, Q_{Al}:

$$Q_{Al}(t) = -A \int_0^t J_A(t)dt = \\ = \frac{AD_A C_{A0}}{l}\left[t - \frac{l^2}{6D_A} + \frac{2l^2}{\pi^2 D_A} \times \sum_{n=1}^{\infty} \frac{(-1)^{n+1}}{n^2} exp\left(-\frac{D_A n^2 \pi^2 t}{l^2}\right)\right] \qquad (14)$$

The permeate pressure is, then, obtained from the amount of species A permeating out of the membrane:

$$p_p(t) = \frac{AD_A p_f}{Vl}\left[t - \frac{l^2}{6D_A} + \frac{2l^2}{\pi^2 D_A} \times \sum_{n=1}^{\infty} \frac{(-1)^{n+1}}{n^2} exp\left(-\frac{D_A n^2 \pi^2 t}{l^2}\right)\right] \qquad (15)$$

where A is the cross-sectional area available for gas penetration perpendicular to the direction of diffusion and V is the volume of the receiving chamber. The steady-state asymptote of Equation 15 is found by taking the limit as $t \to \infty$, reducing the trantient term to zero. The permeate pressure is, then, given by:

$$\lim_{t\to\infty} p_p(t) = \frac{AD_A p_f}{Vl}\left[t - \frac{l^2}{6D_A}\right] \qquad (16)$$

The intercept on the time axis of the plot of pressure rise versus time is defined as the time lag, t_{lag}:

$$t_{lag} = \frac{l^2}{6D_A} \qquad (17)$$

From the time lag and knowing the membrane thickness, the diffusion coefficient can be obtained.

3 Optimization of the gas permeation setup

The gas permeation setup built by Eusébio [15] showed low reproducibility and high uncertainty associated for more permeable membranes, possibly due to various factors such as the small size of the receiving chamber and the fact that the setup wasn´t evacuated with a vaccum pump prior to the measurements. Furthermore, a transient state was not observed in measurements with O_2 and N_2, which made it impossible to determine the diffusion and solubility coefficients for these gases by the time lag method.

With the purpose of obtaining more precise gas permeation measurements of membranes, an increase of the volume of the receiving chamber of Eusébio´s setup was done by adding a second cylinder (Cylinder 2) with a volume of 394.9 ± 1.5 cm^3. Also, a vacuum pump was added to evacuate the whole setup before each measurement in order to abide by the initial and boundary conditions, Equations 11.a, 11.b and 11.c, of the Fick´s Second Law of diffusion. The resulting setup (Setup A) is presented in Figure 1.

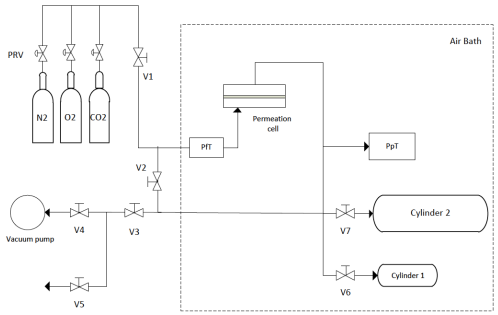

Figure 1 - Schematic representation of the former gas permeation setup (Setup A)

Samples of a commercial membrane, taken from a MBO marketed by Avecor/Medtronics, model 0600, were tested with N_2 in the setup A.

Figure 2 shows the pressure rise in the permeate side with time for the commercial membrane by feeding N_2 at a pressure of 1.9 bar, in setup A with Cylinder 2 of volume 394.9 cm^3. It can be seen that after about 5 seconds, the pressure rises fast and then slows down at about 15 seconds and gradually reaches a steady state. As a result, the time lag, which is the intersection of the steady state asymptote with the time axis, is negative. Furthermore, the resulting N_2 permeance is 2.17 ± 0.21 x 10^{-5} cm^3 cm^{-2} s^{-1} cmHg, which is not in agreement with the previously reported result of 0.33 ± 0.04 x 10^{-5} cm^3 cm^{-2} s^{-1} cmHg obtained by Eusébio´s setup [15]. The occurrence can be explained by the existence of resistance to the transport of gas which prevents its uniform distribution downstream from the membrane leading to a higher concentration of gas near the membrane.

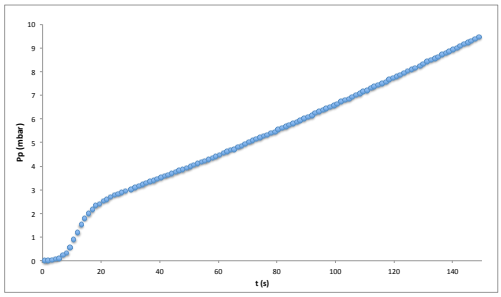

Figure 2 – N_2 permeate pressure vs time for the commercial membrane at a feed pressure of 1.9 bar, obtained in setup B with Cylinder 2 of volume 394.9 cm^3

The big cylinder was substituted by a smaller one with a volume of 167.2 ± 0.2 cm^3.

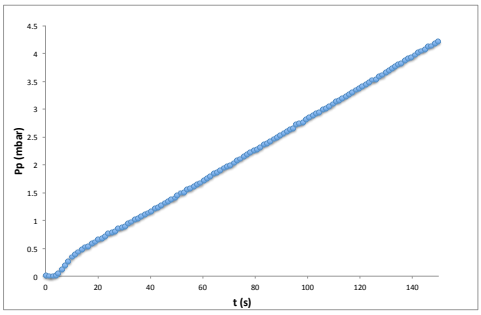

Figure 3 - N_2 permeate pressure vs time for the commercial membrane at a feed pressure of 1.9 bar, obtained in setup A with Cylinder 2 of volume 167.2 cm^3

Observing Figure 3, it can be seen that the pressure still rises fast after 5 seconds and gradually slows down. The time lag is at a value around 0 s. However, the N_2 permeance is 0.34 ± 0.00 x 10^{-5} cm^3 cm^{-2} s^{-1} cmHg, which is in agreement with the previously reported result of 0.33 ± 0.04 x 10^{-5} cm^3 cm^{-2} s^{-1} cmHg [15], which means there was an improvement by substituting the big cylinder, probably beacause its larger volume amplified the effect of the resistance to the gas transport in the tubes.

Kruczek et al. have also observed this situation and have studied various configurations of the permeate and have developed analytical solutions for the calculation of the effective time lag [20,21,22,23].

This situation is expected to occur in high vacuums, which is required by the time lag method, where the transport of gas molecules is governed by the Knudsen flow, which happens when a gas molecule collides much more frequently with the walls of the tube rather than with other gas molecules. This occurs when the radius of the tube (r) is much smaller than the mean free path of gas molecules (λ). It is common to assume that when $r/\lambda < 0.1$, the gas transport is controlled by Knudsen diffusion.

Figure 4 shows the relationship between the mean free path of N_2 molecules at 300 K and the pressure. Using the criterion $r/\lambda < 0.1$, it also shows the pressures below which the Knudsen flow exists in standard stainless steel tubes of 1/8, 1/4 and 1/2 in., with the respective internal diameters of 0.175, 0.386 and 1.02 cm.

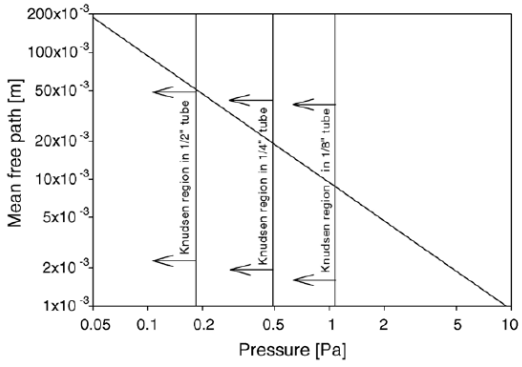

Figure 4 - Effect of pressure on the mean free path of N_2 molecules at 300 K [20]

As the tubes used in the gas permeation setup are of 1/8 in. and according to Figure 4, Knudsen diffusion exists below a pressure of 1 Pa, for N_2 molecules at 300 K. Above this pressure, r/λ increases and the collisions between gas molecules become more frequent and the resistance to accumulation of gas should decrease. However, in this experiment, where the vacuum pump used is capable of reaching pressures below 10 Pa, the resistance to gas transport was observed. Kruczek et al. have also observed that even at initial pressures of 5.5 Pa and higher where the transport is not controlled by the Knudsen diffusion, the effect of the resistance still occured.

As suggested by Kruczek et al., the positions of the pressure transmitter (PpT) and Cylinder 1 were switched as shown in Figure 5 (setup B), so that the pressure transmitter is placed at the end of the main tube.

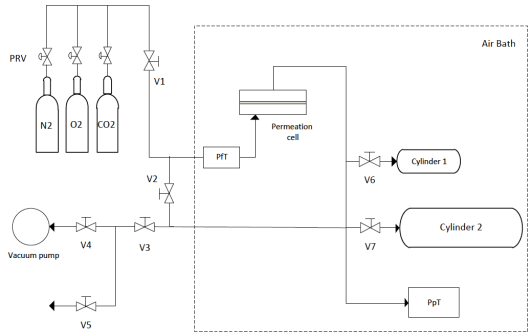

Figure 5 - Schematic representation of the gas permeation setup (Setup B)

In Figure 6 the effect of the resistance to accumulation of gas is no longer shown and it can be seen that in the transient state the pressure gradually rises until reaching the steady state.

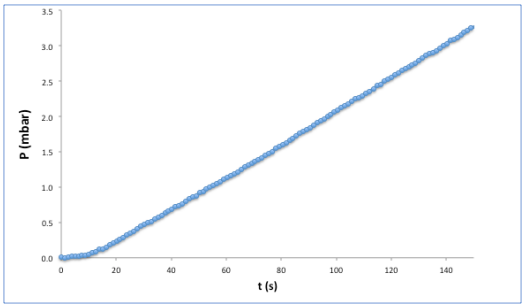

Figure 6 - CO_2 permeate pressure vs time for the A31 membrane at a feed pressure of 1.9 bar, obtained in setup B

The obtained setup (Figure 1) consists of a permeation cell, a feed pressure sensor (PfT) (Setra, Model 205, Massachusetts, USA), a permeate pressure transmitter (PpT) (Intelligent Transmitter Paroscientific, Series 6000, model 6100A-CE Inc. Washington, USA) attached to a Paroscientific model 710 display unit, which is connected to a computer, a small cylinder with a volume of 12.6 ± 0.1 cm^3 (Cylinder 1), a big cylinder with a volume of 167.2 ± 0.2 cm^3 (Cylinder 2) and a vacuum pump (Edwards E2M2 Rotary Vane Vacuum Pump, UK). The volume of Cylinder 1 was previously calibrated by gravimetry [15], in which the cylinder was filled with a liquid of known density and weighted. The calibration of the volumes of Cylinder 2 and the tubes were done by gas expansion. The tubes in the receiving chamber have a volume of 13.5 ± 0.01 cm^3, resulting in a total volume of the permeate side of 193.3 ± 0.3 cm^3.

The membrane is sandwiched between two plates of stainless steel in the permeation cell with a surface area of 9.62 cm^2. The tubbing system contains tubes of stainless steel 316 with an external diameter of 1/8 inch (Hoke®), needle valves (3700 Series, Hoke®) and tube fittings made of stainless steel, titanium and brass (Gyrolok®). The equipment was installed in a thermostatic system which consists of a wine fridge (cold source), a resistance thermometer, a heater connected to a PID controller and a fan to homogenize the inner temperature. The variation of the pressure was recorded with the software Digiquartz® version 2.0 (Paroscientific Inc, Washington, USA).

4 Experimental

4.1 Materials

Two prepolymers were used for the synthesis of the poly(ester urethane urea) membranes: poly(propylene oxide) (PPO) based polyurethane prepolymer with three isocyanate terminal groups (PUR), supplied by Fabrires-Produtos Químicos S.A., and polycaprolactone diol prepolymer (PCL), supplied by Sigma-Aldrich and with a molecular weight of 530 Da. The solvents used were the dimethylformamide (DMF) (p.a. grade, 99.8%) and diethyl ether (DEE) (p.a.

grade, 99.5%) provided by Panreac. The catalyst used was stannous octoate (p.a. grade, 95%) provided by Sigma-Aldrich.

Gas permeation experiments and gas solubility measurements were carried out by using nitrogen (purity ≥ 99.999%), carbon dioxide (purity ≥ 99.98%) and oxygen (purity ≥ 99.5%) supplied by Air Liquide.

4.2 Synthesis of poly(ester urethane urea) membranes

Integral asymmetric poly(ester urethane urea) membranes were synthesized by a modified version of the phase inversion technique. Firstly, two casting solutions were prepared with a PUR/PCL weight ratio of 90/10 and a polymer/solvent weight ratio of 65/35. The ratio of solvents DMF/DEE in each solution was 3/1 and 1/1. 3-4 drops of catalyst, stannous octoate, were added and the solutions were stirred for about 2 hours at room temperature. In the next step, each solution was spread on a glass plate with a 150 µm casting knife and a solvent evaporation time of 1 minute was applied. After this, the glass plates were placed in a coagulation bath (deionized water) for at least 12 hours. The membranes were carefully removed from the glass plate, washed with deionized water to remove all solvents and left to dry at room temperature. The resulting membranes were designated A31 and A11, which correspond to DMF/DEE ratios of 3/1 and 1/1, respectively.

Nonporous symmetric membranes were synthesized with the same casting solutions. After spreading the solutions on the glass plate, they were left to dry for at least 24 hours. Later, they were removed from the glass plate, washed with deionized water and dried at room temperature. These membranes were designated D31 and D11, which correspond to DMF/DEE ratios of 3/1 and 1/1, respectively.

4.3 Gas permeation measurements

The gas permeation experiments on the poly(ester urethane urea) membranes were performed in the optimized setup, as shown in Figure 1, by the constant volume method. This method consists in determining the gas flux through the membrane by measuring the variation of pressure with time in the receiving chamber.

For a given measurement, the membrane is inserted in the cell and the setup is thermostated for at least 3 hours, until it stabilizes at a temperature of 37 ± 0.2 ºC. During this time, the membrane is degassed using the vacuum pump, with valves V1 and V5 closed and all the other valves opened. The volume of the receiving chamber can be chosen by manipulating valves V6 and V7. One gas (N_2, O_2, CO_2) is measured at a time by regulating the respective pressure reducing valve (PRV) to a feed pressures between 1.5 and 4 bar. To start the measurement, valves V2 and V3 are closed and the permeate pressure recording starts when V1 is opened. The feed pressure sensor is monitored to ensure that the feed pressure is constant. The pressure rise in the receiving chamber is recorded automatically at intervals of approximately 1.3 seconds and with a precision better than 10 Pa. After the measurement, V1 is closed and V2 and V3 are opened and the setup is degassed with the vacuum pump for at least 10 minutes before the next measurement. It was verified that this amount of time is enough to degass the membrane as no increase in pressure was observed after closing valve V3.

The average permeances, diffusion and solubility coefficients and respective standard deviations were calculated from the measurements of three excerpts of a membrane.

4.4 Gas solubility measurements by the barometric method

The gas solubility of one of the synthesized membranes, A31, for N_2, O_2 and CO_2 were measured independently by the barometric method, in order to compare the values obtained by the time lag method.

The gas sorption experiments were performed in a volumetric apparatus which method is described in [24]. The membrane was inserted in a cell, placed in the volumetric apparatus and put under high vacuum (Pfeiffer Vacuum, APR 266, vacuum below 10^{-2} Pa) for at least an hour. The apparatus has two chambers that are separated by a valve: one which volume was previously calibrated (chamber 1) and another where the cell is inserted along with the membrane sample (chamber 2), which volume is unknown. Volume calibration was carried out with helium. The measurements were performed at 37.5 ºC, using a water bath, and at pressures up to 4 bar.

The gas is introduced in chamber 1 at a desired pressure, which value is registered. The gas is then expanded to chamber 2 by opening the valve and the pressure decay is monitored until it reaches a constant value (after 30-60 minutes). The final pressure value is registered and the sorbed gas is determined by mass balance. More gas is introduced into the system for the next measurement and this process is repeated until a complete isotherm is obtained.

To prevent contamination of the volumetric apparatus by the solvents used in the membrane synthesis, the membrane was previously put under vacuum in a Schlenk flask, at ambient temperature, for at least a week to ensure that no trace of solvent is left in the membrane.

5 Results and Discussion

5.1 Structure characterization of the membranes by Scanning Electron Microscopy

Integral asymmetric poly(ester urethane urea) membranes A31 and A11 were synthesized with DMF/DEE weight ratios of 3/1 and 1/1, respectively, PUR/PCL weight ratio of 90/10, polymer/solvent ratio of 65/35 and solvent evaporation time of 1 minute. Figures 7a to 7f show the SEM images for the top and bottom surfaces and cross-sections of A31 and A11.

Observing the top surfaces (Figures 7a and 7d), A31 has more pore like features than A11. These pore like features will be referred to as pores in the rest of this work. In terms of size, the pores in A31 are all small and similar in size while A11 presents pores of different sizes and in some areas there are no visible pores. Regarding the bottom surfaces (Figures 7b and 7e), A31 has a porous surface, however, the pores are larger and lower in number compared to the top. The bottom surface of A11 is similar to its top surface. Relatively to the cross-sections (Figures 7c and 7f), a well defined dense layer on the top is not observed, probably because it is below the discrimination level of the technique, however, it can be seen that the pores on the top layer are smaller and larger in number compared to the lower layer.

Nonporous symmetric poly(ester urethane urea) membranes D31 and D11 were synthesized with DMF/DEE weight ratios of 3/1 and 1/1, respectively, PUR/PCL weight ratio of 90/10 and polymer/solvent ratio of 65/35.

Figures 7g to 7l show the SEM images for the top and bottom surfaces and cross-sections of D31 and D11. It can be seen that they are completely dense.

The total thickness of the membranes were measured from the cross-sections SEM images using the software ImageJ. The average thickness and respective standard deviations (σ) are represented in Table 1.

Table 1 - Average thickness and respective standard deviation of the membranes

Membrane	Thickness, l (µm)	σ (µm)
A31	46	0.9
A11	61	0.5
D31	63	0.3
D11	64	0.1

5.2 Gas permeation measurements

N_2, O_2 and CO_2 gas permeation experiments were performed for the poly(ester urethane urea) membranes by the constant volume method, where the pressure rise in the receiving chamber, initially in vacuum, was recorded online, at a temperature of 37 ºC. Figure 8 shows the permeation curves for the

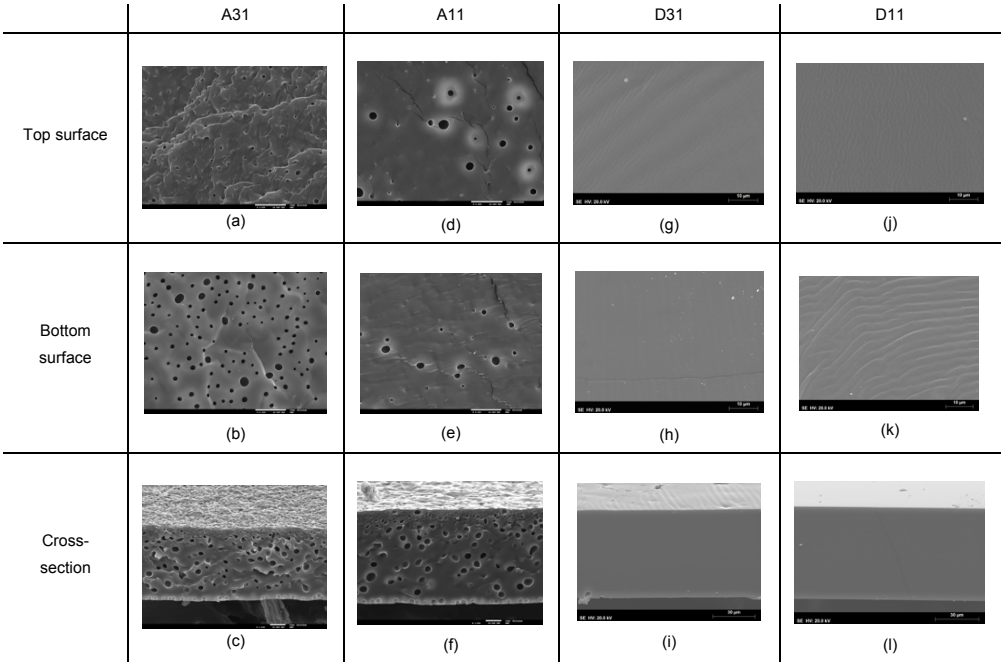

Figure 7 - SEM images of A31: (a) top surface, (b) bottom surface, (c) cross-section; A11: (d) top surface, (e) bottom surface, (f) cross-section; D31: (g) top surface, (h) bottom surface, (i) cross-section; D11: (j) top surface, (k) bottom surface, (l) cross-section

three gases obtained for A31 membrane. Similar permeation curves were obtained for the other membranes.

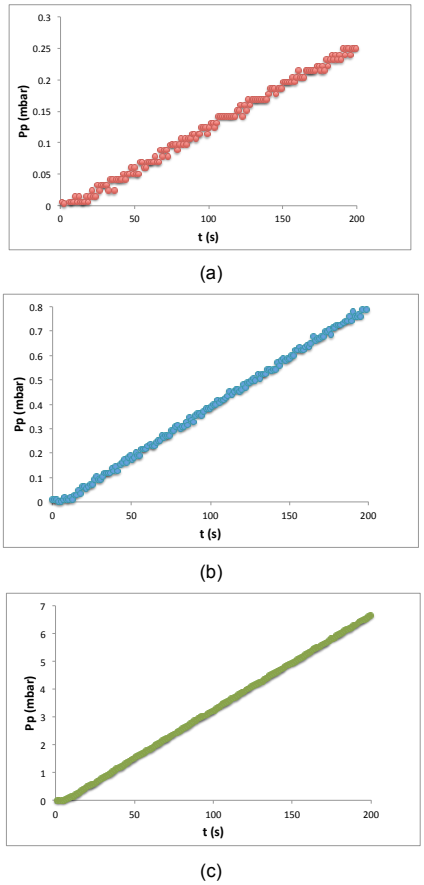

Figure 8 – Permeate pressure vs time for A31 membrane with (a) N_2 at P_f = 2.3 bar, (b) O_2 at P_f = 2.4 bar and (c) CO_2 at P_f = 2.2 bar

In Figure 8, a transient state and a steady state can be distinguished for all three gases. At similar feed pressures, after 200 seconds the permeate pressure increased 0.25, 0.80 and 7.0 mbar for N_2, O_2 and CO_2, respectively.

Figure 9 shows the N_2, O_2 and CO_2 permeation curves for A31 membrane at different feed pressures. From each steady state slope, $\frac{dp_p}{dt}$, a volumetric flux, J, can be obtained.

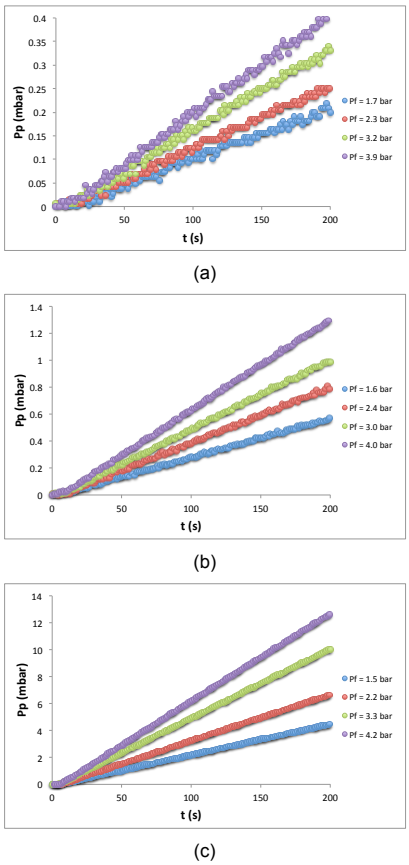

Figure 9 – Permeate pressure vs time for A31 membrane with (a) N_2, (b) O_2 and (c) CO_2 at different feed pressures

Plots of the volumetric fluxes (J) vs the transmembrane pressure (TMP) were obtained for all membranes, as shown in Figure 10. TMP is the difference between the feed pressure and the initial permeate pressure ($TMP = p_f - p_p(t = 0)$), which is approximately 0 mbar.

In Figure 10, similar volumetric fluxes were obtained for all membranes. The volumetric fluxes increase in the order of N_2, O_2 and CO_2.

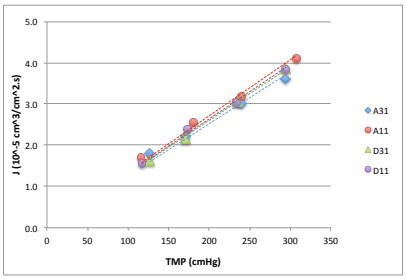

(a)

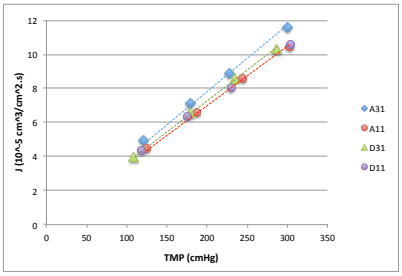

(b)

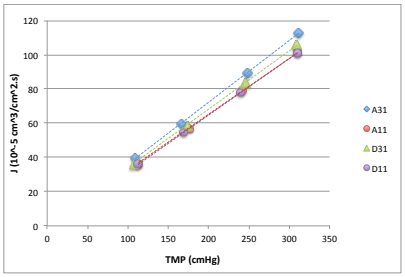

(c)

Figure 10 – (a) N_2, (b) O_2 and (c) CO_2 volumetric fluxes vs the transmembrane pressure for membranes A31, A11, D31 and D11

Table 2 and Figure 11 shows the extrapolated N_2, O_2 and CO_2 volumetric fluxes obtained for membranes A31, A11, D31 and D11 at a feed pressure of 1 bar.

Table 2 - N_2, O_2 and CO_2 volumetric fluxes for membranes A31, A11, D31 and D11 at a feed pressure of 1 bar

Membrane	J_{N_2} (10^{-5} $cm^3/cm^2.s$)	J_{O_2} (10^{-5} $cm^3/cm^2.s$)	J_{CO_2} (10^{-5} $cm^3/cm^2.s$)
A31	0.96 ± 0.14	2.6 ± 0.32	25.8 ± 2.6
A11	0.95 ± 0.01	2.6 ± 0.03	25.1 ± 0.6
D31	0.96 ± 0.04	2.6 ± 0.08	25.5 ± 0.8
D11	0.91 ± 0.04	2.5 ± 0.07	24.0 ± 0.9

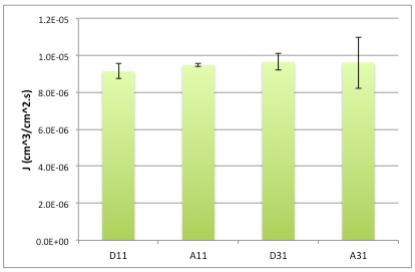

(a)

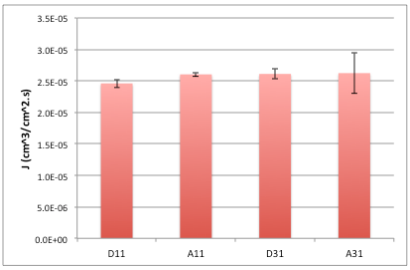

(b)

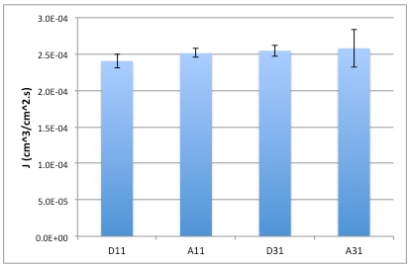

(c)

Figure 11 – (a) N_2, (b) O_2 and (c) CO_2 volumetric fluxes obtained for membranes A31, A11, D31 and D11

The permeances, $Perm$, were obtained from the slopes of the volumetric flux vs TMP plots:

$$Perm = \frac{dJ}{d(TMP)} \left[\frac{cm^3(STP)}{cm^2\ s\ cmHg}\right] \quad (18)$$

The obtained average N_2, O_2 and CO_2 permeances with respective standard deviations for each membrane are shown in Table 3.

Table 3 – Average N_2, O_2 and CO_2 permeances for membranes A31, A11, D31 and D11

Membrane	$Perm_{N_2}$ (10^{-6} $cm^3/cm^2.s.cmHg$)	$Perm_{O_2}$ (10^{-6} $cm^3/cm^2.s.cmHg$)	$Perm_{CO_2}$ (10^{-6} $cm^3/cm^2.s.cmHg$)
A31	0.13 ± 0.02	0.35 ± 0.04	3.4 ± 0.3
A11	0.12 ± 0.00	0.34 ± 0.00	3.3 ± 0.1
D31	0.13 ± 0.01	0.34 ± 0.01	3.4 ± 0.1
D11	0.12 ± 0.01	0.32 ± 0.01	3.2 ± 0.1

The average values of permeances obtained for each gas are similar for all membranes. The CO_2 permeances are approximately 30 times and 10 times higher than the N_2 and O_2 permeances, respectively.

The permeances of the nonporous symmetric membranes were converted to permeability coefficients (P) in Barrer units by the expression below:

$$P = Perm \times l \times 10^{10}\ [Barrer] \quad (19)$$

Table 4 shows the average permeability coefficients of all three gases for the nonporous symmetric membranes and the respective standard deviations.

Table 4 – N_2, O_2 and CO_2 permeability coefficients obtained for membranes D31 and D11

Membrane	P_{N_2} (Barrer)	P_{O_2} (Barrer)	P_{CO_2} (Barrer)
D31	8 ± 0	21 ± 0	208 ± 6
D11	8 ± 0	21 ± 0	202 ± 4

Faria *et al.* [14] have reported P_{CO_2} values between 113 and 337 Barrer and P_{O_2} values between 10 and 11 Barrer for nonporous symmetric membranes containing 0 to 15 weight % PCL. For 10 weight % of PCL, the values of P_{CO_2}

and P_{O_2} were 337 Barrer and 11 Barrer, respectively, which is higher than the P_{CO_2} (208 and 202 Barrer) and lower than the P_{O_2} (21 Barrer) obtained for the nonporous symmetric membranes in this experiment.

In comparison to other membranes of current MBOs, the obtained P_{CO_2} values are higher than the values of PP (9 Barrer) and PMP (90 Barrer) membranes. The obtained P_{O_2} values are in between the values of PP (2 Barrer) and PMP (30 Barrer) membranes [25].

A Membrane Blood Oxygenator (MBO) is required to deliver about 250 cm^3(STP)/min of O_2 and remove about 200 cm^3(STP)/min of CO_2 [4]. The surface area of membrane demanded to meet these requirements was estimated from the obtained volumetric fluxes at a feed pressure of 1 bar, as presented in Table 5.

Table 5 - O_2 and CO_2 volumetric fluxes for membranes A31, A11, D31 and D11 and estimated membrane surface area for MBOs

Membrane	J_{o_2} (10^{-5} $cm^3/cm^2.s$)	Membrane surface area (m^2)	J_{co_2} (10^{-5} $cm^3/cm^2.s$)	Membrane surface area (m^2)
A31	2.6	15.9	25.8	1.3
A11	2.6	16.0	25.1	1.3
D31	2.6	16.0	25.5	1.3
D11	2.5	16.9	24.0	1.4

Due to high CO_2 permeation properties, the MBOs would require a total membrane surface area of approximately 1.3 m^2, which is lower than the membrane surface area of current commercial MBOs, which is approximately 2 m^2 [26]. As for O_2, because of its low permeation properties it would require a total membrane surface area of about 16 m^2 which is inconvenient, as it is an order of magnitude higher than the average membrane surface area of commercial MBOs. However, it should be reminded that these membranes have better hemocompatibility [11], which might make it acceptable to have a MBO with a larger surface area.

5.3 Determination of the diffusion and solubility coefficients

The diffusion and solubility coefficients of the poly(ester urethane urea) membranes were determined by the time lag method. From each permeation curve, a time lag was obtained from the intersection of the steady state asymptote with the time axis.

The diffusion coefficients were calculated using Equation 17 in section 2.2 and the obtained values are shown in Table 6 and Figure 12, along with the average time lags.

Table 6 – N_2, O_2 and CO_2 average time lags, diffusion coefficients and respective standard deviations obtained for membranes A31, A11, D31 and D11

Membrane	$t_{lag_{N_2}}$ (s)	D_{N_2} (10^{-7} cm^2/s)	$t_{lag_{O_2}}$ (s)	D_{O_2} (10^{-7} cm^2/s)	$t_{lag_{CO_2}}$ (s)	D_{CO_2} (10^{-7} cm^2/s)
A31	5.1	7.1 ± 0.6	4.8	7.4 ± 1.4	4.8	7.5 ± 1.4
A11	4.7	12.9 ± 3.2	6.9	8.9 ± 1.6	5.4	11.3 ± 1.9
D31	6.9	9.5 ± 0.9	6.2	10.7 ± 0.7	8.8	12.2 ± 0.5
D11	5.2	13.0 ± 4.0	6.2	11.0 ± 0.5	5.7	11.9 ± 0.6

An ANOVA test was executed to compare the obtained average values of the diffusion coefficients between the membranes. This test is a way to compare means of different groups to see if the differences between them are statistically significant. The test showed that there is a significant difference between them for a confidence level of 95%.

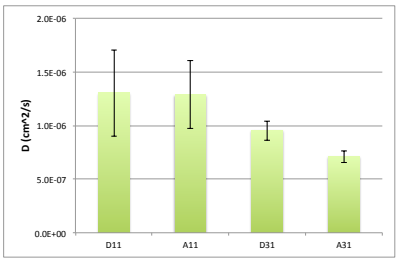

(a)

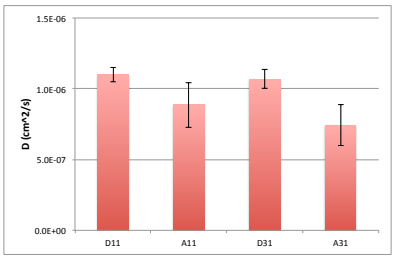

(b)

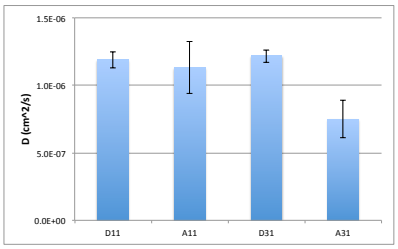

(c)

Figure 12 – (a) N_2, (b) O_2 and (c) CO_2 diffusion coefficients and respective standard deviations obtained for membranes A31, A11, D31 and D11

The solubility coefficients were determined by dividing the permeability coefficients $(Perm \times l)$ by the diffusion coefficients.

Table 7 – N_2, O_2 and CO_2 average solubility coefficients and respective standard deviations obtained for membranes A31, A11, D31 and D11

Membrane	S_{N_2} (10^{-2} cm^3/cm^3cmHg)	S_{O_2} (10^{-2} cm^3/cm^3cmHg)	S_{CO_2} (10^{-2} cm^3/cm^3cmHg)
A31	0.08 ± 0.01	0.25 ± 0.05	2.2 ± 0.2
A11	0.07 ± 0.02	0.25 ± 0.04	1.8 ± 0.3
D31	0.08 ± 0.01	0.22 ± 0.01	1.7 ± 0.1
D11	0.07 ± 0.01	0.20 ± 0.00	1.7 ± 0.1

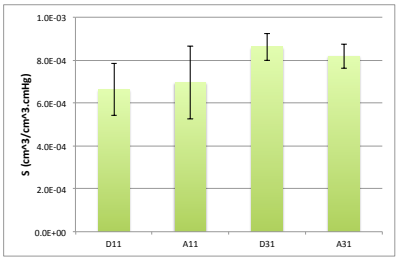

(a)

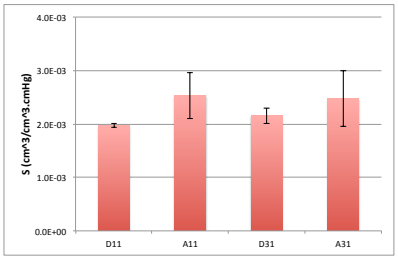

(b)

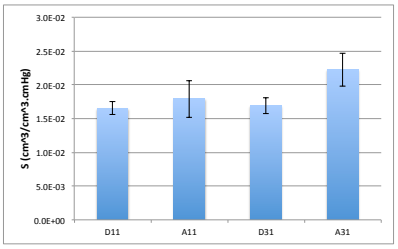

(c)

Figure 13 – (a) N_2, (b) O_2 and (c) CO_2 solubility coefficients and respective standard deviations obtained for membranes A31, A11, D31 and D11

Results from the ANOVA test showed that there is no significant difference between the mean values of N_2 solubilities for a confidence level of 95%, however, the opposite was observed for the mean values of O_2 and CO_2 solubilities.

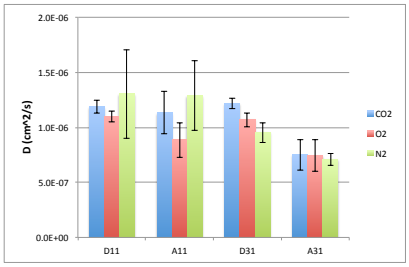

(a)

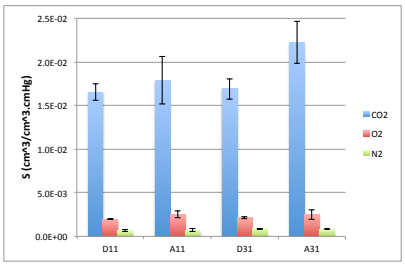

(b)

Figure 14 – (a) Diffusion coefficients and (b) solubility coefficients and respective standard deviations obtained for N_2, O_2 and CO_2 for membranes A31, A11, D31 and D11

As it can be seen in Figure 14, the biggest difference is in the solubility coefficients of the gases in these poly(ester urethane urea) membranes, while not much difference is seen in the diffusion coefficients. Therefore, the solubility is the main contributing factor for the observed difference in permeabilities of the three gases.

Table 8 – N_2, O_2 and CO_2 kinetic diameters and boiling points [27]

Molecule	kinetic diameter (Å)	boiling point (ºC)
CO_2	3.30	-78.5
O_2	3.46	-183
N_2	3.64	-196

Regarding the solubility coefficient, it has been proposed that it is dependant on the gas boiling point or critical temperature [28]. As shown in Table 8, CO_2 has the highest boiling point, which explains its high solubility in the membrane. The boiling points increase in the order of N_2, O_2 and CO_2 and this same trend is observed in the obtained solubility coefficients as shown in Figure 14.

As for the diffusion coefficient, it is known to be dependant on the size of the gas molecule: as the kinetic diameter of the gas molecule increases the diffusion coefficient decreases [28]. From the kinetic diameters shown in Table 8, it would be expected that the diffusion coefficient increases in the order of N_2, O_2 and CO_2. This tendency is observed for membranes D31 and A31 but not for D11 and A11, as shown in Figure 14.

Faria *et al*. [14] have obtained D_{CO_2} and S_{CO_2} values of 8.15 x 10^{-7} cm^2/s and 4.14 x 10^{-2} cm^3/cm^3cmHg, respectively, for membranes containing 10 weight % of PCL, which is in the same order of magnitude as the values obtained in this study.

5.4 Gas solubility measurements by the barometric method

The N_2, O_2 and CO_2 solubilities in membrane A31 were measured by the barometric method in order to compare them to the results obtained from the time lag method. A sorption isotherm was obtained for each gas up to a pressure of 4 bar, as shown in Figure 15.

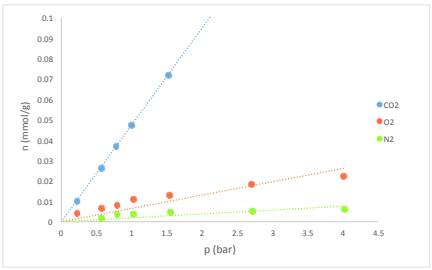

Figure 15 – N_2, O_2 and CO_2 sorption isotherms obtained for membrane A31

It can be seen in Figure 15 that the O_2 and N_2 isotherms show some deviation to the fitted line, possibly because these gases are sorbed by the membrane in very low quantities, which are at the limit of application of the used apparatus. The solubility was obtained from the slope of each isotherm, assuming the validity of Henry´s Law, and is represented as a horizontal line in Figure 16.

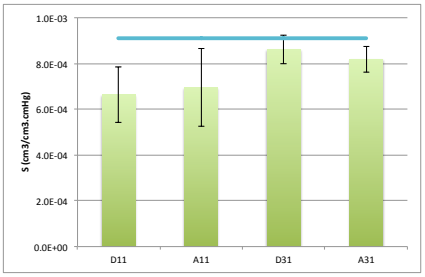

(a)

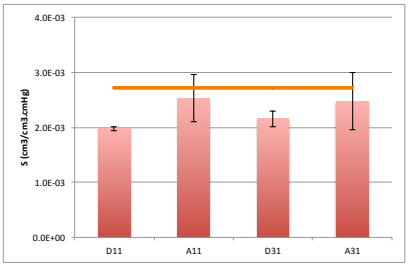

(b)

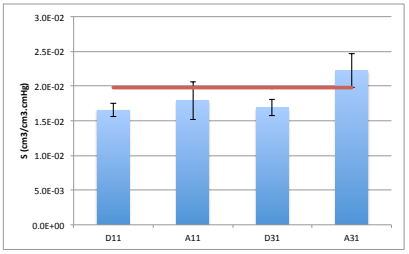

(c)

Figure 16 – (a) N_2, (b) O_2 and (c) CO_2 solubility coefficients obtained for membranes A31, A11, D31 and D11 by the time lag method in comparison with the solubility coefficient obtained by solubility measurement of A31 (horizontal line)

As shown in Figure 16, the solubilities obtained by the barometric method agree with the results obtained by the time lag method, within the experimental uncertainty. This validates the measurements obtained in the current gas permeation setup.

6 Conclusions

The gas permeation setup was optimized by increasing the volume of the receiving chamber and performing vacuum to the setup before the measurements in order to obtain more precise results. A non-negligible resistance to gas transport was observed during measurements as a consequence of the Knudsen flow, which affected the results of permeances and time lags. The effect of the resistance ceased after substituting the big cylinder with volume of 394.9 ± 1.5 cm^3 for a smaller one with volume of 167.2 ± 0.2 cm^3 and placing the pressure transmitter at the end of the main tube. Overall, the current gas permeation setup, with a receiving chamber with a total volume of 193.3 ± 0.3 cm^3, is capable of measuring, at constant temperature, the permeate pressure rise online in the receiving chamber at intervals of 1.3 seconds and with a precision better than 10 Pa, providing highly reproducible results of permeances. Additionally, a transient state was observed for N_2, O_2 and CO_2, which permited the application of the time lag method for the determination of the diffusion and solubility coefficients.

Integral asymmetric poly(ester urethane urea) membranes A31 and A11 were synthesized by a modified version of the phase inversion technique with DMF/DEE weight ratios of 3/1 and 1/1, respectively, PUR/PCL weight ratio of 90/10, polymer/solvent ratio of 65/35 and solvent evaporation time of 1 minute. SEM images revealed that the asymmetry is more noticeable in the membrane A31 than A11, as the difference in the average pore size between the top and bottom layers is bigger and the polymer surface area coverage is smaller in the bottom compared to the top. However, a well defined dense layer on the top is not observed, probably because it is below the discrimination level of the technique. The measured total thickness for A31 and A11 were 46 µm and 61 µm, respectively.

Nonporous symmetric poly(ester urethane urea) membranes D31 and D11 were synthesized by the solvent evaporation technique with DMF/DEE weight ratios of 3/1 and 1/1, respectively, PUR/PCL weight ratio of 90/10 and polymer/solvent ratio of 65/35. SEM images showed them to be completely dense. The measured total thickness for D31 and D11 were 63 µm and 64 µm, respectively.

Similar permeances were obtained for the integral asymmetric and nonporous symmetric membranes: 0.12-0.13x10^{-6} cm^3/cm^2scmHg for N_2, 0.32-0.35x10^{-6} cm^3/cm^2scmHg for O_2 and 3.2-3.4x10^{-6} cm^3/cm^2scmHg for CO_2. The permeability coefficients obtained for the symmetric membranes were: 8 Barrer for N_2, 21 Barrer for O_2 and 202 Barrer (D11) and 208 Barrer (D31) for CO_2.

The membranes showed great CO_2 permeation properties, resulting in an estimated eventual requirement of less membrane surface area than the one of current commercial MBOs, which is approximately 2 m^2. However, it showed low O_2 permeation properties, which would require a total membrane surface area of about 16 m^2. Although it may be inconvenient, these membranes have better hemocompatibility which may compensate for its larger area.

The diffusion coefficients obtained by the time lag method were: 7.1-13.0x10^{-7} cm^2/s for N_2, 7.4-11.0x10^{-7} cm^2/s for O_2 and 7.5-12.2x10^{-7} cm^2/s for CO_2. The solubility coefficients obtained were: 0.07-0.08x10^{-2} cm^3/cm^3cmHg for N_2, 0.20-0.25x10^{-2} cm^3/cm^3cmHg for O_2 and 1.7-2.2x10^{-2} cm^3/cm^3cmHg for CO_2. From these results it can be concluded that the solubility is the main contributing factor for the difference in permeabilities of the three gases. Therefore, gas permeation properties, particularly of O_2, may be improved by enhancing the solubility coefficients.

The solubilities obtained by the barometric method were 0.09x10^{-2} cm^3/cm^3.cmHg for N_2, 0.27x10^{-2} cm^3/cm^3.cmHg for O_2 and 1.98x10^{-2} cm^3/cm^3.cmHg for CO_2, which are in agreement with the values obtained by the time lag method, within the experimental uncertainty, which validates the measurements obtained in the current gas permeation setup.

7 Bibliography

[1] G. P. Gravlee, R. F. Davis, J. W. Hammon, and B. D. Kussman, *Cardiopulmonary Bypass and Mechanical Support - Principles and practice*, 4th ed.: Wolters Kluwer, 2015.

[2] A. M. Gaffney, S. M. Wildhirt, M. J. Griffin, G. M. Annich, and M. W. Radomski, "Extracorporeal life support," *BMJ*, vol. 431, pp. 982-986, 2010.

[3] T. Yeager and S. Roy, "Evolution of Gas Permeable Membranes for Extracorporeal Membrane Oxygenation," *Artificial Organs*, vol. 41, no. 8, pp. 700-709, 2017.

[4] D. F. Stamatialis et al., "Medical applications of membranes: Drug delivery, artificial organs and tissue engineering," *Journal of Membrane Science*, vol. 308, pp. 1-34, 2008.

[5] D. Palanzo et al., "Evolution of the Extracorporeal Life Support Circuitry," *Artificial Organs*, vol. 34, no. 11, pp. 869-873, 2010.

[6] C. T. Zhao and M. N. de Pinho, "Design of polypropylene oxide/polybutadiene bi-soft segment urethane/urea polymer for pervaporation membranes," *Polymer*, vol. 40, pp. 6089-6097, 1999.

[7] D. P. Queiroz and M. N. de Pinho, "Gas permeability of polypropylene oxide/polybutadiene bi-soft segment urethane/urea membranes," *Desalination*, vol. 145, pp. 379-383, 2002.

[8] D. P. Queiroz, M. N. de Pinho, and C. Dias, "ATR-FTIR studies of poly(propylene oxide)/polybutadiene bi-soft segment urethane/urea membranes," *Macromolecules*, vol. 36, pp. 4195-4200, 2003.

[9] D. P. Queiroz and M. N. de Pinho, "Structural characteristics and gas permeation properties of polydimethylsiloxane/poly(propylene oxide) urethane/urea bi-soft segment membranes," *Polymer*, vol. 46, pp. 2346-2353, 2005.

[10] M. Faria, V. Geraldes, and M. N. de Pinho, "Surface characterization of asymmetric bi-soft segment poly(ester urethane urea) membranes for blood oxygenation medical devices," *International Journal of Biomaterials*, vol. 2012, p. e376321, 2012.

[11] M. Faria, P. Brogueira, and M. N. de Pinho, "Sub-micron tailoring of bi-soft segment asymmetric polyurethane membrane surfaces with enhanced hemocompatibility properties," *Colloids and Surface B: Biointerfaces*, vol. 86, pp. 21-27, 2011.

[12] M. N. de Pinho, "Process of synthesis asymmetric polyurethane based membranes with hemocompatibility characteristics and membranes obtained by said process," US9181384B2, 2010.

[13] M. Faria, M. Rajagopalan, and M. N. de Pinho, "Tailoring bi-soft segment poly(ester urethane urea) integral asymmetric membranes for CO2 and O2 permeation," *Journal of Membrane Science*, vol. 387-388, pp. 66-75, 2012.

[14] M. Faria and M. N. de Pinho, "Phase segregation and gas permeation properties of poly(urethane urea) bi-soft segment membranes," *European Polymer Journal*, vol. 82, pp. 260-276, 2016.

[15] T. M. Eusébio, "Polyurethane urea membranes for membrane blood oxygenators: synthesis and gas permeation properties," Instituto Superior Técnico, 2017.

[16] A. F. Ismail, K. C. Khulbe, and T. Matsuura, *Gas separation Membranes - Polymeric and inorganic*, 1st ed.: Springer International Publishing, 2015.

[17] M. Mulder, *Basic Principles of Membrane Technology*, 2nd ed.: Springer, 1996.

[18] R. M. Barrer and E. K. Rideal, "Permeation, diffusion and solution of gases in organic polymers," *Transactions of the Faraday Society*, vol. 35, 1939.

[19] S. W. Rutherford and D. D. Do, "Review of Time Lag Permeation Technique as a Method for Characterisation of Porous Media and Membranes," *Adsorption*, vol. 3, pp. 283-312, 1997.

[20] B. Kruczek, H. L. Frisch, and R. Chapanian, "Analytical solution for the effective time lag of a membrane in a permeate tube collector in which Knudsen flow regime exists," *Journal of Membrane Science*, vol. 256, pp. 57-63, 2005.

[21] B. Kruczek, F. Shemshaki, S. Lashkari, R. Chapanian, and H. L. Frisch, "Effect of a resistance-free tank on the resistance to gas transport in high vacuum tube," *Journal of Membrane Science*, vol. 280, pp. 29-36, 2006.

[22] S. Lashkari, B. Kruczek, and H. L. Frisch, "General solution for the time lag of a single-tank receiver in the Knudsen flow regime and its implications for the receiver´s configuration," *Journal of Mmebrane Science*, vol. 283, pp. 88-101, 2006.

[23] S. Lashkari and B. Kruczek, "Effect of resistance to gas accumulation in multi-tank receivers on membrane characterization by the time lag method. Analytical approach for optimization of the receiver," *Journal of Membrane Science*, vol. 360, pp. 442-453, 2010.

[24] V. K. Saini, M. L. Pinto, and J. Pires, "Synthesis and adsorption properties of micro/mesoporous carbon-foams prepared from foam-shaped sacrificial templates," *Materials Chemistry and Physics*, vol. 138, pp. 877-885, 2013.

[25] D. N. Gray, "Polymeric Membranes for Artificial Lungs," in *Polymeric Materials and Artificial Organs*, Charles G. Gebelein, Ed., 1984, vol. 256, pp. 151-162.

[26] F. Wiese, K. V. Peinemann, and S. P. Nunes, *Membranes for Artificial Lungs in Membranes for the Life Sciences, Chapter 2.*: Wiley-VCH Verlag GmbH & Co. KGaA, 2007.

[27] R. H. Perry and D. W. Green, *Perry´s Chemical Engineers´Handbook*, 7th ed.: McGraw-Hill, 1997.